ISSN 1392-1320 MATERIALS SCIENCE (MEDŽIAGOTYRA). Vol. 29, No. 2. 2023

Room-temperature Compressive Creep Behavior of Ti-6Al-4V ELI Alloys with a Basketweave Microstructure under Alternating Compressive Stresses

Hao HUANG, Yu ZHANG, Jiafei LU, Zhenhua DAN *, Hui CHANG, Lian ZHOU

College of Materials Science and Engineering & Tech Institute for Advanced Materials, Nanjing Tech University, Nanjing 211816, China

https://doi.org/10.5755/j02.ms.31914

Received 22 July 2022; accepted 26 October 2022

Titanium alloys have great potential as candidate materials for deep-sea facilities. Long-term creep deformation behavior of the pressure-bearing structures made of titanium alloys under alternating compressive stress has a direct impact on structural stability. The compressive creep evaluations of Ti-6Al-4V extra low interstitial (ELI) alloys with basketweave microstructure under alternating stresses have been carried out by a uniaxial compressive creep tester. The compressive creep deformations have strong stress sensitivity due to the larger creep strain by the higher applied compressive stress. The dislocation densities in α and β phases increase with the increase of applied compressive stresses. The dislocation slip and dislocation multiplication occur in α phases accompanied by high dislocations density in β phases caused by compressive deformation. The large strain concentration occurs at the grain boundaries of α/β phase due to dislocation plug after creep, which causes the grain boundary pinning. The compressive creep deformation of Ti-6Al-4V ELI alloys under alternating stress is a decelerating creep process and controlled by <a> dislocation slip. The slight refinements of the grains and hardening have been confirmed after creep. The synergistic effects of dislocation multiplication, grain boundary pinning and grain refinements lead to strengthening the Ti-6Al-4V ELI alloys and decelerating the compressive creep.

Keywords: Ti-6Al-4V ELI alloy, alternating stress, compressive creep, dislocation slip, dislocation multiplication.

1. INTRODUCTION

In the last several decades, many scholars paid extensive attention to the high-temperature tensile creep of titanium alloys due to the increasing demands in the aerospace fields. The high-temperature tensile creep undergoes three stages until the tensile fractures including the primary creep stage, steady-state creep stage and accelerated creep stage [1]. Viswanathan et al. [2] have reported that the creep deformation of Ti-6Al-2Sn-4Zr-2Mo alloys at 538 °C and 565 °C under constant load is mainly controlled by dominant dislocation climbing and minor dislocation slip. The high-temperature creep of different types of titanium alloys is controlled by thermal diffusion and the dislocation climbing dominates the creep deformation [3]. In recent years, room-temperature tensile creep has attracted more attention. However, dislocation climbing and atomic thermal diffusion become difficult due to the lack of enough activation energy at room temperature. Therefore, room-temperature creep generally includes only the primary creep stage with high deformation rates and steady-state creep stage with minimum creep rates [4, 5]. The tensile creep tests on commercially pure titanium (Grade 2) alloys with different stress levels under medium and low temperatures conducted by Chang et al. [6] show strong stress sensitivity and nonnegligible tensile creep deformation. The steady-state creep behaviors with minimum creep rates have been found in the room-temperature creep [7 – 9]. Oberson et al. [10] investigated the tensile creep behavior of α-Ti alloys and found that dislocation slip and twinning dominate the room-temperature tensile creep. Zhang et al. [11] studied the tensile creep behavior of Ti-36Nb-2Ta-3Zr-0.35O at room temperature and found the creep saturation phenomenon at the applied tensile stresses lower than the yield strength.

The development of deep-sea marine engineering has increasingly attracted the attention all over the world. The building materials for the deep-sea facilities are required to meet the requirements of mechanical properties and corrosion resistance due to a variety of corrosive media in the deep seas. Titanium alloys have been selected as one of the preferred materials for the pressure-bearing structures of large deep-sea equipments due to high strength-to-weight ratio, superior corrosion resistance and good weldability [12, 13]. The room-temperature compressive creep of the industrial pure titanium TA2 conducted by Zhang et al. [14] has a threshold stress and its phenomenological compressive creep constitutive equation has been established to be in form of the Norton equation. The creep behavior and structural deformation of the pressure hulls under the interaction of the high hydrostatic pressure in the deep sea determine the service life, safety and the reliability of the equipment. Few reports related to the high-pressure compressive creep behavior and creep mechanisms of titanium alloys at a temperature of 2 – 35 °C have been delivered until now. Chen [15] has discussed the high-pressure compressive creep behavior and phenomenological Norton constitutive equation of Ti-6Al-3Nb-2Zr-1Mo alloy and Ti-6Al-4V extra low interstitial (ELI) alloys under uniaxial constant compressive stress through uniaxial

*Corresponding author. Tel.: +86-25-83587270.
E-mail: *zhenhuadan@njtech.edu.cn* (Z. Dan)

compressive creep tester. Wang et al. [16] carried out the creep experiments of Ti-6Al-4V ELI alloys with duplex and basketweave microstructure under different compressive stress levels at room temperature environments. After constant stress creep, the dislocation densities in the α phases increase sharply and many dislocations are entangled, and the creep deformation is mainly caused by dislocation slip in α phases. The constant compressive creep and creep mechanism of Ti-6Al-4V alloys with different microstructures were discussed by Lu et al. [17, 18]. The compressive creep occurs beyond the stress threshold and the compressive creep behavior is controlled by dislocation slip. The chemical composition and macro-texture of Ti-6Al-4V alloys, creep stress level and pre-plastic-strain also affect the room temperature creep behavior [19, 20]. The studies above mentioned conclude the phenomenological Norton constitutive equations as their prediction models for compressive creep.

Some researchers related to alternating-stress creep of stainless steels [21], copper alloys [24] and other superalloys [23, 24] have been reported. Both the cross-slip of screw dislocation segments and the rearrangement of trapped dislocations in walls cooperate to produce the enhanced creep rate during the cyclic loading/unloading of AISI 316L stainless steels [21]. The higher creep rates occur under the cyclic creep for copper single crystals, particularly one-order increase of the creep rates after the prolonged durations [22]. Meanwhile, the negative linear dependency between static creep rates and creep time has been broken instead of the fast increase of cyclic creep rates after 100 min of the cyclic creep [22]. The faster creep rates than those under constant stress and constant creep plasticity of DZ17G superalloys under different loading conditions at 870 °C have been reported [25]. Xie et al. [24] conducted static, cyclic durability and dynamic creep tests on Fe-based and Ni-based alloys and the shorter fracture life of cyclic durability, faster creep rates and worse creep resistance during cyclic loading/unloading creep tests have been confirmed in comparison to these under the constant stresses. Moreover, the dislocation densities keep increasing and dislocation slip dominates the creep deformations during the entire cyclic creep. There are few researchers on the alternating-stress creep of titanium alloys. The deep-sea facilities, such as Jiaolong submersible and ocean scientific vessels, suffer complicated stress distributions during diving and floating operations. The different effects of the alternating, rapid alternating and other stress modes on the strain hardening, the change of the creep rates and creep mechanisms possibly take place. The compressive creep behavior of the pressure hulls thus becomes more complicated. It is of particular importance to investigate the high-stress compressive creep of titanium alloys under periodic alternating stress in the deep-sea environment.

The fatigue crack growth rate of the titanium alloys with the basketweave microstructure is the lowest and the comprehensive mechanical properties of the basketweave microstructure are also excellent. The creep resistance of the basketweave microstructure is stronger than that of the duplex microstructure, which can better meet the high fatigue requirements for long life in the fields of aerospace and deep-sea equipment. The compressive creep mechanism of titanium alloys in the deep-sea environment with corrosive media at $2-4$ °C is to be studied. The basic compressive creep constitutive equation is established by using the room temperature compressive creep without considering the action of the corrosive medium and then the influence of the corrosive medium and the change of the stress levels on the compressive creep is established to expand the constitutive equation. The creep rates and microstructure evolutions under the interaction of the alternating stress differ from those under constant stress. Therefore, the effect of different alternating stresses on the room-temperature compressive creep behavior and microstructure changes of Ti-6Al-4V ELI alloys with basketweave microstructure is to be investigated from the aspects of the creep strains, hardening, dislocation multiplication and grain refinements. The creep deformation mechanism under the alternating compressive stress of $803-1104$ MPa aim to be clarified on the basis of the microstructural evolution related to stress concentration measured by Electron Back-scatter Diffraction, dislocation multiplication and dislocation slip analyzed by X-ray diffractometer and transmission electron microscopy and the Norton constitutive equations from the stress sensitivities.

2. EXPERIMENTAL PROCEDURE

Ti-6Al-4V ELI alloys with basketweave microstructure were obtained from Baoti Co. Ltd. The Ti-6Al-4V ELI alloys have fabricated by vacuum melting, forging and heat treatment with the chemical composition (wt.%) of 6.1Al, 4.2V, 0.23Fe, 0.04C, balanced Ti. The creep specimens were machined into cylinders with a length of 70 mm and a diameter of 20 mm. Based on mechanical properties test results, the compressive yield strength, ultimate strength and elongation of Ti-6Al-4V ELI alloys are 1003 MPa, 1817 MPa and 29.2 %. [15]. The uniaxial high-stress compressive creep testers were used to perform the alternating creep experiments at 803 MPa ($0.8R_{pc0.2}$), 903 MPa ($0.9R_{pc0.2}$) and 1104 MPa ($1.1R_{pc0.2}$) at room temperature. The deep-sea equipment will be in a state of diving and floating during operation and the stress mode of the alternating stress is shown in Fig. 1. The stress was linearly increased to the setting compressive stress and kept constant compressive stress for 500 h and then unloaded for 50 h. Three creep cycles were carried out under each compressive stress level. The metallographic characteristics were observed on the mirror-polished specimens etched with Kroll's solution (HF 1 ml, HNO_3 2 ml and H_2O 7 ml) by using optical microscopy (OM, Zeiss Observer A1m, Zeiss). The grain size of the microstructure was measured by Nano Measurer software over 150 grains. The phase contents were analyzed by X-ray diffraction with a CuKα radiation with a scanning angle from 30° to 90° and a scanning rate of 10°/min. to quantitatively analyze the dislocation densities, the samples after creep were measured by XRD with a scanning rate of 1°/min in 2Θ from 30° to 40°. For EBSD analysis, the samples before and after creep were ground on SiC sandpaper with grits from 240# to 3000# and then the samples were electro-polished in a solution of 5 % perchloric acid and 95 % ethanol at a voltage of 40 V using an electric polishing machine (Struers Lectropol-5). The EBSD observation was performed on a

scanning electron microscope equipped with an EBSD detector (SEM/EBSD JEOL JMS-7001F). The thin disk (Φ3 mm) with a thickness of about 60 μm was used for ion milling in a solution of 180 ml methanol, 105 ml butanol and 15 ml perchloric acid at an accelerating voltage of 200 kV. The morphology and dislocation structures of the crept samples at 903 MPa were analyzed by transmission electron microscopy (TEM, Tecnai-G220). The microhardness was measured by a micro-Vickers apparatus under a load of 200 g.

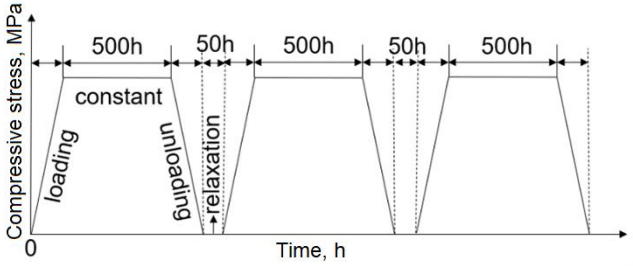

Fig. 1. Schematic change of alternating stress during the creep experiments

3. RESULTS AND DISCUSSION

3.1. Effect of alternating compressive stress on compressive creep behavior

The strain-time curves of Ti-6Al-4V ELI alloys with basketweave microstructure under alternating creep at 803, 903 and 1104 MPa as shown in Fig. 2. During the loading of the compressive stress, the strain increases gradually and reaches a platform. The creep deformation increases significantly with the increase of the applied compressive stress. The compressive creep at three compressive stresses underwent both the primary creep stage and the steady-state creep stage without the appearance of the accelerated creep stage. The total strain in the first compression cycle reaches 0.9 % at 803 MPa, 1.8 % at 903 MPa and 3.1 % at 1104 MPa, respectively. In the subsequent cycles, the total strain is slightly higher than that in the first cycle. Under the low applied compressive stress of 803 MPa, the creep deformation behavior is not obvious, and the total strain is less than 1.5 %. In the second creep cycle, the compressive stress resulted in a total strain of 1.87 %, which was about twice of that at 803 MPa. During unloading, the strain of Ti-6Al-4V ELI alloys compressed at 1104 MPa decreases significantly from 3.13 % to 1.34 % in the first cycle, and those at lower stress changed similarly down to about 0.3 %.

The power-law equation has been used to fit the strain-time data in the following form:

$$\varepsilon = At^m, \quad (1)$$

where ε is the strain; A is the time constant; t is the creep time and m is the creep exponent. The values of m are obtained from the slope of the fitting lines of the strain-time curves at steady states by using Eq. 1. In many cases, m value can be considered as a criterion of the stress sensitivity of creep [15, 16]. The dependent relationship of the steady-state creep rates and the m values on the applied compressive stresses and cycle times is shown in Fig. 3. The steady-state creep rates are the largest in the first cycle and increase from 2.51×10^{-10} s^{-1} to 15.8×10^{-10} s^{-1} as the increase of the compressive stress from 803 MPa to 1104 MPa. The steady-state creep rate decreases from 7.26×10^{-10} s^{-1} in the first cycle to 3.53×10^{-10} s^{-1} in the third cycle. Meanwhile, the creep rates decrease with the increase of the cycle numbers. The m value changes similarly with the creep rates here. The m values change from 0.013 at 803 MPa to 0.058 at 1104 MPa and decrease from 0.033 to 0.004 with the increase of the cycle numbers at the compressive stress of 903 MPa. The linear dependency shown in Fig. 3 indicates that the creep deformation during alternating compressive creep exhibits stress-dependent sensitivity. Based on Eq. 1 and the creep data above mentioned, the compressive creep has typical deceleration creep characteristics under alternating compressive stress. The steady-state creep rate tends to the minimum creep rate and fracture failure does not occur.

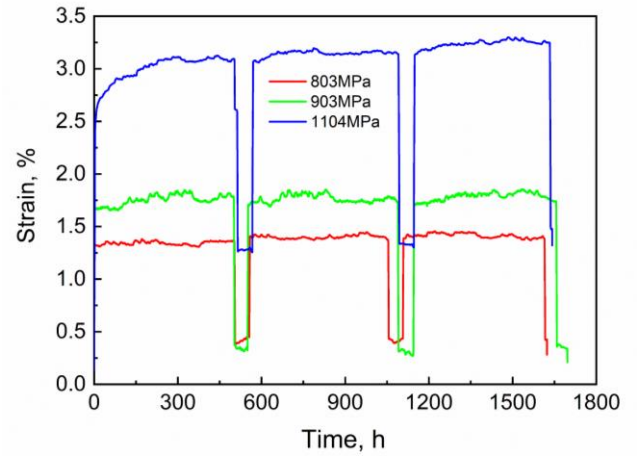

Fig. 2. Strain-time curves of Ti-6Al-4V ELI alloys with basketweave microstructure at different alternating stresses

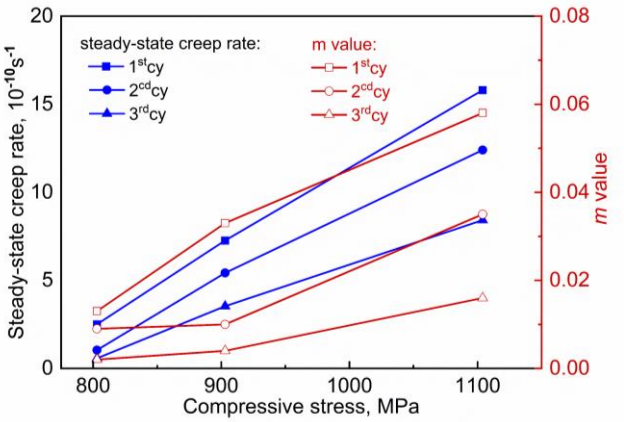

Fig. 3. Steady-state creep rate and m value of Ti-6Al-4V ELI alloys with basketweave microstructure at different alternating stresses

The stress-strain hysteresis loops of the first cycle at 803, 903 and 1104 MPa are shown in Fig. 4. When the compressive stress is applied, the Ti-6Al-4V ELI cylinder samples underwent elastic deformation, compression under static stress and recovery during unloading. The presence of the linear part in the stress-strain hysteresis loops indicates the elastic strain during loading. When the compressive stress reaches the static state, compressive creep occurs with

the extension of the duration time. Parallelogram-shaped stress-strain curves indicate that the Ti-6Al-4V ELI alloys with basketweave microstructure have a good ability for deformation and recovery. The accumulated strain increases with the compressive stress in the same cycle. It is worth noting that there is a strain accumulation platform under constant stress holding, which indicates that creep behavior appears. Comparing the strain at the different applied compressive stresses, it is found that alternating compressive creep behavior becomes more significant with the increase of applied compressive stresses. The deformation strain during the constant stress for 500 h is mainly contributed by the creep deformation and will not recover during relaxation. The strain generated under the constant compressive stress is thus close to the creep strain here. The stress-strain curves of the subsequent cycles are like the first cycle with smaller strains.

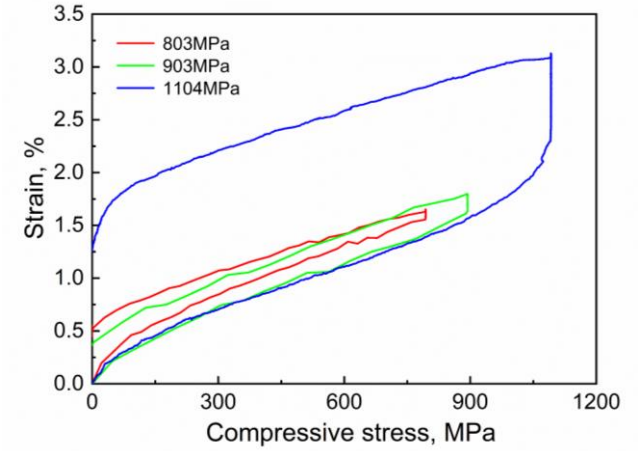

Fig. 4. Hysteresis loops of Ti-6Al-4V ELI alloys with basketweave microstructure at different alternating stresses

Parallelogram-shaped stress-strain loops in one whole cycle are obtained and the enclosed area can be used to calculate the strain energy density. The creep strain during alternating compressive creep is calculated by the steady state creep rates obtained from Fig. 2. Both the strain energy density and creep strain of Ti-6Al-4V ELI alloys under different alternating stresses and different cycle times are summarized in Fig. 5. In the first cycle, the creep strain is 0.79 % at 1104 MPa. The compressive yield strength has not been exceeded at the applied stresses of 803 and 903 MPa and the compressive creep is a decelerating creep process. Therefore, the creep strain of Ti-6Al-4V ELI alloys at 803 and 903 MPa is all very low. The creep strain decreases significantly with the cycle numbers under the same applied compressive stress. The creep strain at 1104 MPa decreased to 0.12 in the second cycle and 0.06 % in the third cycle. The calculated creep strains are close to the strain at the constant stress for 500 h in Fig. 4. With the increase of the applied compressive stresses, the strain energy densities in the same cycle increase and are the largest in the first creep cycle. With the increase of applied compressive stresses from 803 MPa to 1104 MPa, the strain energy density increases sharply from 1.6 MJ m^{-3} to 15.54 MJ m^{-3} during the first cycle. The largest strain energy density in the first cycle indicates the main deformation takes place in the first cycle and the deformation by the compressive stress becomes more difficult. The mechanism for the deceleration creep of the Ti-6Al-4V ELI alloys during alternating cyclic creep is deserved to be clarified from the aspects of the microstructure changes during cyclic creep, such as strain hardening by the dislocation multiplication and grains refinement during compression.

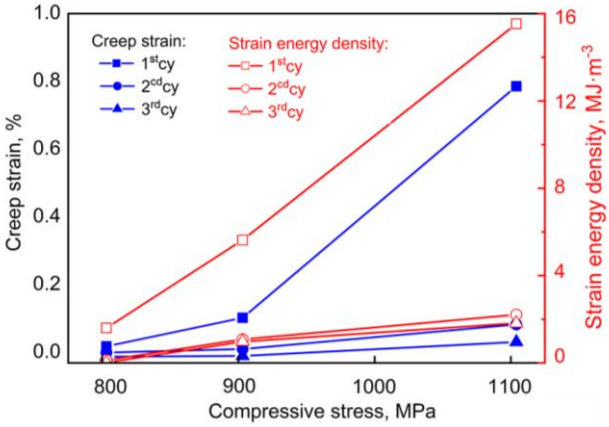

Fig. 5. Creep strain and strain energy density of Ti-6Al-4V ELI alloys with basketweave microstructure under different alternating stresses and cycle numbers

3.2. Effect of compressive creep deformation on microstructure characteristics

The crystalline characteristics affected by compressive creep have been analyzed by XRD. The XRD patterns of Ti-6Al-4V ELI alloys with basketweave microstructure before and after creep as shown in Fig. 6 a. The diffraction peaks at 2θ of 35.1°, 38.2°, 40.2°, 53°, 63°, 71° and 77° correspond to $(10\bar{1}0)$, (0002), $(10\bar{1}1)$, $(10\bar{1}2)$, $(11\bar{2}0)$, $(10\bar{1}3)$ and $(11\bar{2}2)$ planes of the hcp α phase and the peak at 2θ = 39.3° corresponds to the (110) plane of the bcc β phase except for these overlapped diffraction peaks with α phase. The c/a ratio of Ti-6Al-4V ELI alloys before and after creep is 1.5957, 1.5949, 1.5938 and 1.5935, respectively. The value of the c/a ratio decreases with the increase of applied compressive stresses. These changes indicate that the crystal cells have been compressed to a smaller level, which demonstrates the lattice strain take place after compression. These lattice strains might further result in hardening by decreasing the c/a ratio [25]. Moreover, the dislocation multiplication and slip in titanium alloys play an important role in macroscopic creep behavior. The full width at half maximum half-width (FWHM) of XRD can be used to calculate the change of dislocation densities after the compressive creep [26]. Dunn and Koch have proposed a formula [27] for calculating the dislocation densities using FWHM:

$$\rho = \frac{\beta^2}{4.35b^2}, \quad (2)$$

where ρ is the dislocation density; β is the FWHM; b is the Burgers. The XRD patterns of the crept samples between 38° and 40° were measured at a rate of 1°/min and the change of dislocation densities before and after creep was analyzed by XRD diffraction peaks of α (0002) and β (110) planes in Fig. 6 b and c.

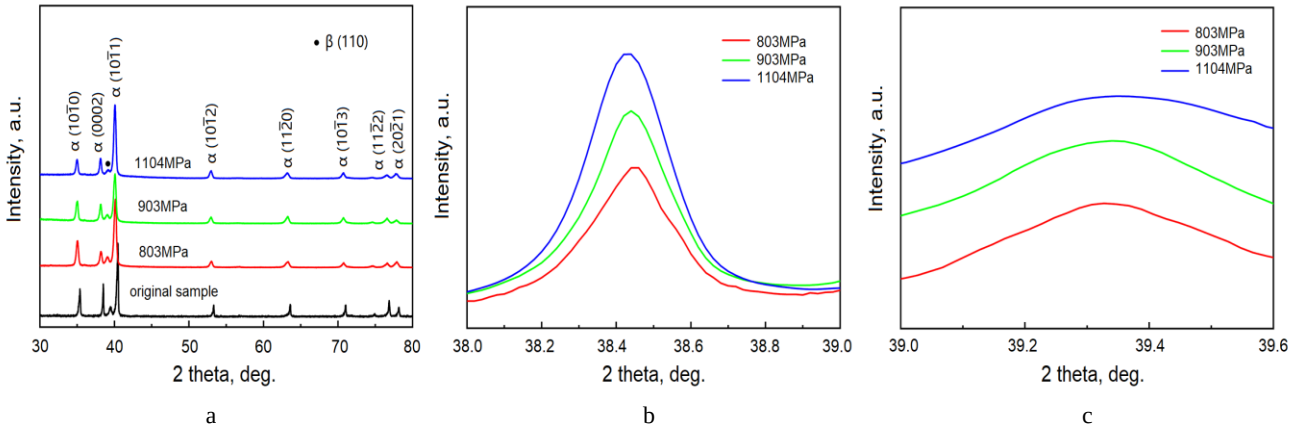

a b c

Fig. 6. XRD patterns of Ti-6Al-4V ELI alloys: a – with basketweave microstructure before creep; b – after creep from α (0002) plane; c – after creep from β (110) plane

During the creep process of titanium alloys, the dislocations are mainly a-type dislocation sliding on the (0002) basal plane [27]. The dislocation densities of α (0002) and β (110) planes of Ti-6Al-4V ELI alloys with basketweave microstructure after alternating creep calculated by Eq. 2 are listed in Table 1. Basing of FWHM of α (0002) crystal plane, the dislocation densities of α phases after creep at 803, 903 and 1104 MPa are 5.85×10^{13}, 7.10×10^{13} and 7.65×10^{13} m^{-2}, respectively. The dislocation densities increase dramatically with the increase of the applied compressive stresses. The slight change of dislocation densities of the β phase indicates that a large number of dislocations are formed in the β phase at the initial compressive stage. It is due to the bcc crystal of β phase bcc structure easy to generate dislocation under compressive stresses. The results indicate that dislocation multiplication mainly occurs in the α phase and dislocation multiplication possibly strengthens the α phase, which causes the hardening with the increase of applied compressive stresses [28]. The tendency of the change of dislocation densities is consistent with that of total strain and creep strain in Fig. 2 – Fig. 5.

Table 1. The dislocation density of α (0002) and β (110) planes of Ti-6Al-4V ELI alloys with basketweave microstructure after alternating creep

Planes	Compressive stress, MPa	Dislocation density, 10^{13} m^{-2}
α (0002)	803	5.85
	903	7.10
	1104	7.65
β (110)	803	5.57
	903	5.73
	1104	5.78

The metallographic structures of Ti-6Al-4V ELI alloys with basketweave microstructure before and after creep are shown in Fig. 7. According to Fig. 7 a, the Ti-6Al-4V ELI alloys consist of intertwined lamellar α and β phases showing the characteristics of basketweave microstructure. The average width of α grains of the alloys before compressive creep is about 3.6 μm. The optical photographs of Ti-6Al-4V ELI alloys with basketweave microstructure after creep at 803, 903 and 1104 MPa are shown in Fig. 7 b and d. There are no obvious morphological changes in the microstructure before and after creep. However, the width of α grains decreases with the increase of applied compressive stresses based on the statistical analysis by Nanomeasure® software. The widths of α grains are 2.8, 2.2 and 1.9 μm under alternating creep at 803, 903 and 1104 MPa, respectively. Compared with the width of α grains before creep, the width of α grains is reduced by 20 %, 37.7 % and 46.2 % after the alternating creep of 3 cycles at 803, 903 and 1104 MPa, respectively.

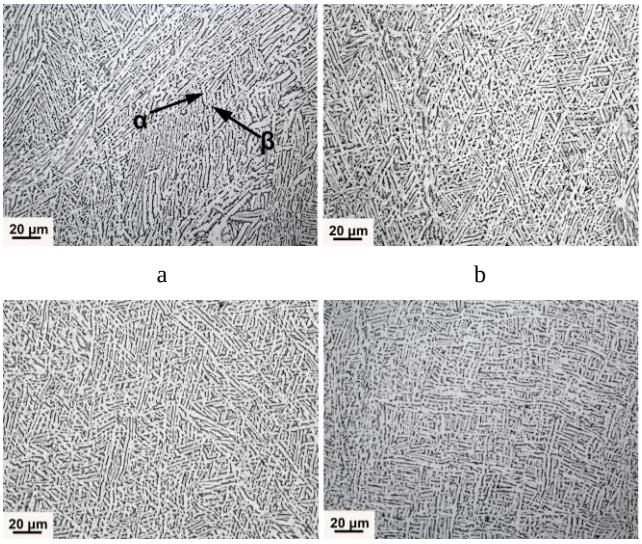

a b

c d

Fig. 7. Optical metallographic structures of Ti-6Al-4V ELI alloys with basketweave microstructure: a – before creep; b – after creep at 803 MPa; c – after creep at 903 MPa; d – after creep at 1104 MPa

Fig. 8 shows the TEM images of Ti-6Al-4V ELI alloys with basketweave microstructure before and after creep at 903 MPa. It can be seen in Fig. 8 a that the alloy is a duplex microstructure including bright white α phase and dark black β phase. The dislocation densities are low and a few dislocations are concentrated at the α/β phase boundary. These dislocations are probably caused by the residual stress during sample processing. The TEM image of the alloy after alternating creep at 903 MPa is shown in Fig. 8 b. The dislocation densities of the α phases significantly increase in comparison to that before creep. A series of parallel linear

dislocations can be seen in the α phase and a similar dislocation structure has been also found in previous studies [29]. The dislocation multiplications are achieved after compression. The generated dislocations begin to slip in the α phases. A large number of dislocation slips occur in the α phases and form a partial dislocation network. The slip system is activated in multiple directions, as marked by g1 and g2 in Fig. 8 b. This is consistent with the conclusions of XRD and the creep deformation is mainly controlled by the movement of dislocations in the α phases [30]. As shown in Fig. 8 b, a large number of dislocations accumulate at the α/β phase boundary, which leads to dislocation entanglement. These dislocation plugs pin at phase boundaries and grain boundaries during the compressive creep process.

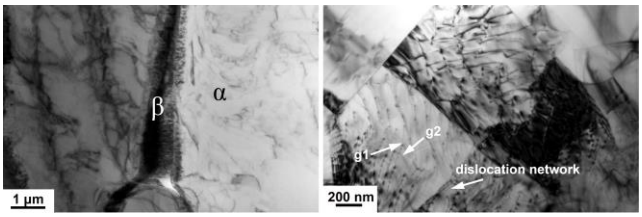

a b

Fig. 8. Bright images of Ti-6Al-4V ELI alloys with basketweave microstructure: a – before creep; b – after creep at 903 MPa

According to the $\vec{g}\cdot b = 0$ invisibility criterion, the types of dislocation can be distinguished [3]. Fig. 9 a and b show the bright field images and corresponding diffraction patterns along the $<2\bar{1}\bar{1}0>_\alpha$ zone axis. The diffraction spots (0002), $(01\bar{1}0)$ and $(01\bar{1}2)$ corresponding to the base plane, prism plane and pyramidal plane are calibrated in Fig. 9 b, respectively. When the operating reflection is $\vec{g} = [01\bar{1}0]$, the bright field images and corresponding diffraction patterns are shown in Fig. 9 c and d. As seen in Fig. 9 c, the <c> dislocation is invisible and there are many <a> dislocations and a few <c+a> dislocations. Similarly, when the operating reflection is $\vec{g} = [0002]$, the bright field images and corresponding diffraction patterns are shown in Fig. 9 e and f. According to Fig. 9 e, the <a> dislocation is invisible and there are only a few <c+a> dislocations. By comparing with Fig. 9 c and e, it can be seen that the <a> dislocations are mainly generated in the alloys after creep at 903 MPa. In addition, the crystal planes of dislocation slip are calibrated in Fig. 9 c and e and the <a> dislocations generated are mainly base plane slip on (0002) plane after alternating creep at 903 MPa.

The inverse pole diagrams and KAM diagrams of Ti-6Al-4V ELI alloys with basketweave microstructure before and after creep are shown in Fig. 10. The inverse pole diagrams and KAM diagrams in Fig. 10 can be used to analyze the misorientation and the strain distribution at the phase boundaries. Fig. 10 a reflects the misorientation of the original alloys. It can be seen that the lamellar α phases in different directions are interlaced to form a basket shape. These α phases may be formed in the same β phase grain during heat treatment, so the grain orientation is the same. The α phase is dominated by (0001) orientation before creep.

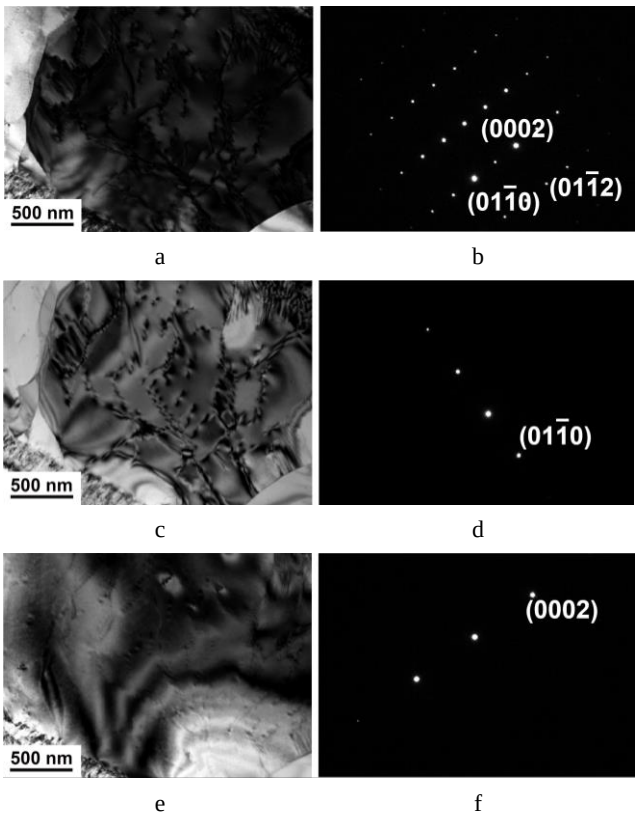

a b

c d

e f

Fig. 9. TEM micrographs of Ti-6Al-4V ELI alloys: a, c, e – with basketweave microstructure; b, d, f – corresponding electron diffraction pattern after creep at the alternating compressive stress of 903 MPa

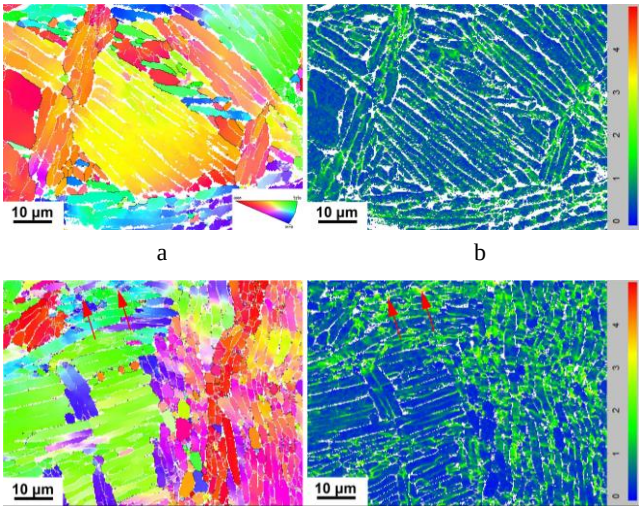

a b

c d

Fig. 10. IPF (a, c) and KAM (b, d) of Ti-6Al-4V ELI alloys: a, b – with basketweave microstructure before creep; c, d – after creep at 903 MPa

In Fig. 10 b, most areas are dark blue and the value of KAM is around 0.2 %. The strain distribution in the sample is relatively uniform and only a small amount of stress concentration exists at the grain boundary and dislocation densities are low. The inverse pole diagrams and KAM diagrams of Ti-6Al-4V ELI alloys with basketweave microstructure after creep at 903 MPa are shown in Fig. 10 c and d. It can be seen that grain orientation has

changed and there are a large number of lamellar α phases with grain orientation of $(\bar{1}2\bar{1}0)$. It can be determined that the orientation change is mainly due to the accumulation of a large number of dislocations in the lamellar α phase, resulting in deflection and torsion in local areas [31]. Compared with Fig. 10 b, the bright green area increased significantly and a large strain concentration occurs inside the grain with the orientation of $(\bar{1}2\bar{1}0)$. The KAM value of the yellow or red region marked by the red arrow is larger than 3 %. As presented in Fig. 5, the creep strain is only 0.79 in the first cycle and 0.06 in the third cycle. According to the value of KAM before and after creep, the compressive creep has strain concentration within the range of characteristic region under alternating stress. By comparing the orientations of corresponding positions in Fig. 10 a and c, it can be found that stress concentration mainly occurs at the high-angle trigonal grain boundary. The distribution of the creep deformation mainly resulted from the deformation of these high-strain regions in the α phases. On the other hand, the average grain sizes of the α phases have been analyzed by EBSD. The average grain sizes of α grains are confirmed to be 4.72 μm before creep and 3.72 μm after creep at 903 MPa. The distribution ratios of the grains with a size of 5 – 10 μm and over 10 μm decrease from 7.9 % and 3.9 % down to 2.4 % and 1.1 %. This is consistence with the experimental results in Fig. 7, although there are some differences in the sizes. Therefore, the compressive creep causes grain refinement.

The changing tendency of the microhardness, the width of the α grains by OM, the reciprocal of the square roots of the widths of the α grains by OM and the grain sizes by EBSD are plotted in Fig. 11. It can be seen that the microhardness increases significantly with the increase of applied compressive stresses. The microhardness of Ti-6Al-4V ELI alloys with basketweave microstructure before creep is 303 $HV_{0.2}$ and the microhardness after creep at 903 MPa is 348 $HV_{0.2}$, which is about 15 % higher than that before creep. The changes in the width of α grains obtained by OM and EBSD indicate that α grains are deformed and refined. The slope of the microhardness versus applied compressive stress is confirmed to 0.079, and that of the reciprocal of the square roots of the widths of the α grains verses the applied compressive stress is done to 0.0008. Both fitted lines have the same changing tendency. The increase of the microhardness proves the occurrence of the hardening from the increase of the dislocation density. This phenomenon may be attributed to the microstructural changes, such as dislocation multipli-cation and grain refinement before and after compressive creep.

3.3. Discussion

The significant decreases of the creep strain and steady-state creep rates of Ti-6Al-4V ELI alloys with basketweave microstructure with the increase of cyclic times during the alternating creep process in Fig. 2 – Fig. 5 are attributed to the effects of dislocation multiplications, dislocation pinning, grain refinement and hardening during the compressive creep process. The strain and creep strain increase significantly with the increase of external compressive stress, as shown in Fig. 2 and Fig. 4. The dislocation depletion theory proposed by Marschall [32] points out that the constant-stress creep in the first alternating cycle is a depletion process of movable dislocation sources. When dislocation slip encounters phase boundaries or other obstacles, dislocations plug up and stop moving [22, 32]. As the creep deformation in the subsequent creep cycles continues, the movable dislocations are gradually exhausted. During the process of reloading, a small amount of new movable dislocations are generated and a few remaining movable dislocations continue to slip under the action of applied stress. Eventually, the dislocations plug up again and become stationary dislocations [14]. Creep deformation becomes slow, so the steady-state creep rate and creep strain decrease. The XRD analysis of dislocation multiplication (Fig. 6) and distribution features of the experiment data by TEM calibration (Fig. 8) show that slip system in multiple directions is activated and the new moving dislocations are generated. Moreover, a large number of dislocations entangle at the grain boundary and phase boundary. The dislocations are finally pinned by the grain boundaries. The increase of creep deformation rates is inhibited and the creep strains and creep rates are eventually reduced under the effect of dislocation strengthening grain boundaries [33]. The dislocation multiplication, dislocation pinning and hardening contribute to the strengthening of the Ti-6Al-4V ELI alloys and the microhardness of Ti-6Al-4V ELI alloys increases during the compressive creep deformation.

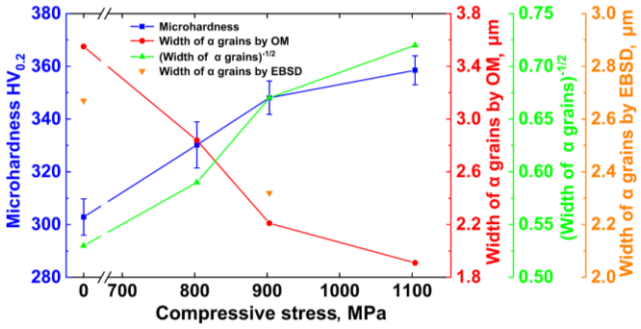

Fig. 11. Dependency of the microhardness, the width of α grains and the reciprocal of the square roots of the widths of the α grains by OM and the width of α grains by EBSD of Ti-6Al-4V ELI alloys with basketweave microstructure before and after creep

On the other hand, the widths of α grains are reduced by 37.7 % under alternating creep at 903 MPa compared with the width of α grains before creep in Fig. 7. The grains are refined to a certain extent during the compression. According to the Hall-Petch law, the strength of the alloys increases after grain refinement. At the same time, the microhardness of Ti-6Al-4V ELI alloys after the alternating compressive creep in Fig. 11 increases after the compressive creep. The strain and creep strain cause the strain hardening [6, 25]. The recovery softening and strain hardening form a balance and the steady-state creep occurs during the compressive creep [34]. The c/a ratio of hcp Ti changes and the restricted dislocation motion affects the hardening of the Ti [35], which has the same with the shrinkage of the a crystal cells shown in Fig. 6. The resistance to creep deformation increases with the accumulation of cycle times. The creep rates in the subsequent cycles are reduced due to

the increase of the strength improved by the strain hardening. As shown in Fig. 2 and Fig. 3, the creep strain and the *m* value of compressive creep index decrease with the increase of creep time. According to the results stated above, the creep rate and the *m* value of the compressive creep index decrease during alternating compressive creep under the synergistic effect of dislocation multiplication, dislocation pinning, grain refinement and strain hardening (Fig. 3, Fig. 5, Fig. 7, Fig. 8 and Fig. 10). As a result, the decelerating creep appears in Fig. 2.

4. CONCLUSIONS

The alternating compressive creep experiments of Ti-6Al-4V ELI alloys with basketweave microstructure at 803, 903 and 1104 MPa were carried out at room temperature. The alternating compressive creep behavior and the creep deformation mechanism were systematically investigated by XRD, optical microscopy, EBSD and TEM methods. The main conclusions obtained are listed as follows:

1. The Ti-6Al-4V ELI alloys with basketweave microstructure only exist primary creep stage and steady-state creep stage during the alternating compressive creep at room temperature. The compressive creep deformation of Ti-6Al-4V ELI alloys has stress sensitivity.
2. The dislocations generated are mainly a series of straight dislocations and the slip systems are activated in multiple directions after alternating creep. The dislocation slip and dislocation multiplication occur in the α phases. More stress concentration and deflection occur in local regions of lamellar α phases after alternating creep. Compressive creep deformation is mainly controlled by <a> dislocation under alternating stress.
3. The synergistic effects of grain fragments, dislocation multiplication, dislocation pinning and hardening decelerate the compressive creep deformation under the alternating compressive stress.

Acknowledgments

This work is financially supported by The National Key R&D Program of China (2022YFB3705500), Open Project of Taihu Laboratory of Deep-Sea Technology Science (2022JBGS01005) and Key Research and Development Plan of Jiangsu Province (BE2019119). This work is partially supported by Priority Academic Program Development of Jiangsu Higher Education Institution (PAPD).

REFERENCES

1. **Gollapudi, S., Satyanarayana, D.V.V., Phaniraj, C., Nandya, T.K.** Transient Creep in Titanium Alloys: Effect of Stress, Temperature and Trace Element Concentration *Materials Science and Engineering A* 556 2012: pp. 510 – 518. https://doi.org/10.1016/j.msea.2012.07.020
2. **Viswanathan, G.B., Karthikeyan, S., Hayes, R.W., Millsa, M.J.** Creep Behavior of Ti-6Al-2Sn-4Zr-2Mo: II. Mechanisms of Deformation *Acta Materialia* 50 (20) 2002: pp. 4965 – 4980. https://doi.org/10.1016/S1359-6454(02)00280-X
3. **Nie, X., Liu, H., Zhou, X.Z., Yi, D.Q., Huang, B.Y., Hu, Z., Xu, Y.F., Yang, Q., Wang, D.C., Gao, Q.** Creep of Ti-5Al-5Mo-5V-1Fe-1Cr Alloy with Equiaxed and Lamellar Microstructures *Materials Science & Engineering: A*651 2016: pp. 37 – 44. https://doi.org/10.1016/j.msea.2015.10.092
4. **Peng, J., Zhou, C.Y., Dai, Q., He, X.H.** The Temperature and Stress Dependent Primary Creep of CP-Ti at Low and Intermediate Temperature *Materials Science and Engineering A* 611 2014: pp. 123 – 135. https://doi.org/10.1016/j.msea.2014.05.094
5. **Liu, X., Zhang, Q.Q., Zhao, X.C., Yang, X.R., Luo, L.** Ambient-temperature Nanoindentation Creep in Ultrafine-grained Titanium Processed by ECAP *Materials Science and Engineering A* 676 2016: pp. 73 – 79. https://doi.org/10.1016/j.msea.2016.08.111
6. **Chang, L., Zhou, C.Y., Peng, J., Li, J., He, X.H.** Creep Behavior of CP-Ti TA2 at Low Temperature and Intermediate Temperature *Rare Metal Materials and Engineering* 46 (6) 2017: pp. 1463 – 1468. https://doi.org/10.1016/S1875-5372(17)30147-9
7. **Neeraj, T., Hou, D.H., Daehn, G.S., Mills, M.J.** Phenomenological and Microstructural Analysis of Room Temperature Creep in Titanium Alloys *Acta Materialia* 48 (6) 2000: pp. 1225 – 1238. https://doi.org/10.1016/S1359-6454(99)00426-7
8. **Barkia, B., Doquet, V., Couzinié, J.P., Guillot, I.** Room-temperature Creep and Stress Relaxation in Commercial Purity Titanium-influence of the Oxygen and Hydrogen Contents on Incubation Phenomena and Aging-induced Rejuvenation of the Creep Potential *Materials Science and Engineering A* 624 2015: pp. 79 – 89. https://doi.org/10.1016/j.msea.2014.11.073
9. **Gerland, M., Lefrance, P., Doquet, V., Sarrazin-Baudoux, C.** Deformation and Damage Mechanisms in An α/β 6242 Ti Alloy in Fatigue, Dwell-fatigue and Creep at Room Temperature. Influence of Internal Hydrogen *Materials Science and Engineering A* 507 (1 – 2) 2009: pp. 132 – 143. https://doi.org/10.1016/j.msea.2008.11.045
10. **Oberson, P.G., Ankem, S.** The Effect of Time-dependent Twinning on Low Temperature (<0.25 * Tm) Creep of An Alpha-titanium Alloy *International Journal of Plasticity* 25 (5) 2009: pp. 881 – 900. https://doi.org/10.1016/j.ijplas.2008.06.002
11. **Zhang, W., Liu, Y., Wu, H., Lan, X.D., Qiu, J.W., Hu, T., Tang, H.P.** Room Temperature Creep Behavior of Ti-Nb-Ta-Zr-O Alloy *Materials Characterization* 118 2016: pp. 29 – 36. https://doi.org/10.1016/j.matchar.2016.05.001
12. **Gorynin, I.V.** Titanium Alloys for Marine Application *Materials Science and Engineering A* 263 (2) 1999: pp. 112 – 116. https://doi.org/10.1016/S0921-5093(98)01180-0
13. **Dong, J.J., Fan, L., Zhang, H.B., Xu, L.K., Xue, L.L.** Electrochemical Performance of Passive Film Formed on Ti-A-Nb-Zr Alloy in Simulated Deep Sea Environments *Acta Metallurgica Sinica* 33 (4) 2019: pp. 1 – 10. https://doi.org/10.1007/s40195-019-00958-4
14. **Zhang, M.Y., Gu, B.Q., Tao, J.H.** Prediction Model for Room Temperature Compressive Creep of Commercially Pure Titanium TA2 *Materials for Mechanical Engineering* 42 (12) 2018: pp. 73 – 76.

15. **Chen, B.W.** High Pressure Compressive Creep Behavior of Ti80 and Ti-6Al-4V ELI Alloys at Ambient Temperature. Nanjing, Nanjing Tech University, 2017.
16. **Chen, B.W., Huang, J., Dan, Z.H., Chang, H., Ding, Y., Zhou, L.** Study on High Pressure Compressive Creep Behavior at Ambient Temperature of Ti-6Al-3Nb-2Zr-1Mo Alloy *Hot Working Technology* 47 (24) 2018: pp. 73 – 75. https://doi.org/10.14158/j. cnki. 1001-3814. 2018. 24. 017
17. **Wang, L., Qu, P., Li, Y., Huang, J.H., Wan, Z.Q.** Theoretical and Experimental Investigations for Creep Properties of Titanium Alloy Materials *Journal of Ship Mechanics* 22 (4) 2018: pp. 464 – 474. https://doi.org/10.3969/j.issn.1007-7294.2018.04.009
18. **Lu, J.F., Dan, Z.H., Chen, B.W., Dong, Y.C., Zhang, A.F., Chang, H., Zhou, L.** Research Progress of High Stress Induced Compression Creep of Titanium Alloys *Materials China* 38 (11) 2019: pp. 1074 – 1081. https://doi.org/10.7502/j.issn.1674-3962.201905021
19. **Dan, Z.H., Lu, J.F., Chang, H., Qu, P., Zhang, A.F., Fang, Z.G., Dong, Y.C., Wang, Y., Zhou, L.** High-stress Compressive Creep Behavior of Ti-6Al-4V ELI Alloys with Different Microstructures *Matec Web of Conferences* 321 2019: pp. 11007. https://doi.org/10.1051/matecconf/202032111007
20. **Xi, G.Q., Qiu, J.K., Lei, J.F., Ma, Y.J., Yang, R.** Room Temperature Creep Behavior of Ti-6Al-4V Alloy *Chinese Journal of Materials Research* 35 (12) 2021: pp. 881 – 892.
21. **Deng, T.S., Cao, W., Yang, K.M., Shen, J.X.** Compressive Creep Behavior of Ti-6Al-4V-xSi-ySc Alloys under High Pressure at Room Temperature *Materials Research Express* 9 (4) 2022: pp. 046511. https://doi.org/10.1088/2053-1591/ac6655
22. **Gaudin, C., Feaugas, X.** Cyclic Creep Process in AISI 316L Stainless Steel in Terms of Dislocation Patterns and Internal Stresses *Acta Materialia* 52 (10) 2004: pp. 3097 – 3110. https://doi.org/10.1016/j.actamat.2004.03.011
23. **Kitagawa, K., Toyomoto, O.** Plastic Deformation of Copper Single Crystals under Cyclic Loading *Materials Science and Engineering A* 234 – 236 1997: pp. 591 – 593. https://doi.org/10.1016/s0921-5093(97)00328-6
24. **Yuan, C., Guo, J., Yang, H.** Cyclic Creep Behavior of Directionally Solidified Nickel-base Superalloy DZ17G *Acta Metallurgica Sinica* 35 (9) 1999: pp. 942 – 947.
25. **Dawson, P.R., Boyce, D.E., Park, J.S., Wielewski, E., Miller, M.P.** Determining the Strengths of HCP Slip Systems Using Harmonic Analyses of Lattice Strain Distributions *Acta Materialia* 144 2018: pp. 92 – 106. https://doi.org/10.1016/j.actamat.2017.10.032
26. **Oh, J.M., Lee, B.G., Cho, S.W., Lee, S.W., Choi, G.S., Lim, J.W.** Oxygen Effects on the Mechanical Properties and Lattice Strain of Ti and Ti-6Al-4V *Metals and Materials International* 17 (5) 2011: pp. 733 – 736. https://doi.org/10.1007/s12540-011-1006-2
27. **Dunn, C.G., Kogh, E.F.** Comparison of Dislocation Densities of Primary and Secondary Recrystallization Grains of Si-Fe *Acta Metallurgica* 5 (10) 1957: pp. 548 – 554. https://doi.org/10.1016/0001-6160(57)90122-0
28. **Cserti, J., Tichy, G., Vitek, V.** Stress Effect on Dislocation Motion in BCC Crystal *Solid State Phenomena* 572 (35 – 36) 1993: pp. 545 – 550. https://doi.org/10.4028/www.scientific.net/SSP.35-36.545
29. **Shi, R., Nie, Z.H., Fan, Q.B., Wang, F.C., Zhou, Y., Liu, X.** Correlation between Dislocation-density-based Strain Hardening and Microstructural Evolution in Dual Phase TC6 Titanium Alloy *Materials Science and Engineering A* 715 2018: pp. 101 – 107. https://doi.org/10.1016/j.msea.2017.12.098
30. **Miller, W.H., Chen, R.T., Starke, E.A.** Microstructure, Creep, and Tensile Deformation in Ti-6Al-2Nb-1Ta-0.8Mo *Metallurgical and Materials Transactions A* 18 (8) 1987: pp. 1451 – 1468. https://doi.org/10.1007/BF02646658
31. **Hayes, R.W., Viswanathan, G.B., Mills, M.J.** Creep Behavior of Ti-6Al-2Sn-4Zr-2Mo: I. The Effect of Nickel on Creep Deformation and Microstructure *Acta Materialia* 50 (20) 2002: pp. 4953 – 4963. https://doi.org/10.1016/S1359-6454(02)00279-3
32. **Xu, T.** Phase-transformation Behaviors and Microstructure Control of the High-strength TB8 Alloys. Shanxi, Northwestern Polytechnical University, 2016.
33. **Blum, W., Eisenlohr, P.** Dislocation Mechanics of Creep *Materials Science and Engineering A* 510 2008: pp. 7 – 13. https://doi.org/10.1016/j.msea.2008.04.110
34. **Anderson, S., Collen, B., Kuylenstierna, U., Magneli, A.** Phase Analysis Studies on the Titanium-oxygen System *Acta Chemica Scandinavica* 11 (10) 1957: pp. 1641 – 1652. https://doi.org/10.3891/acta.chem.scand.11-1641
35. **Rusakova, A.V., Lubenets, S.V., Fomenko, L.S., Moskalenko, V.A.** Structural Homogeneity of Nanocrystalline VT1-0 Titanium. Low-temperature Micromechanical Properties *Low Temperature Physics* 38 (10) 2012: pp. 980 – 988. https://doi.org/10.1063/1.4758787